Thin film-based colorful radiative cooler using diffuse reflection for color display

Junren Wen[1†], Xiao Chen[2†], Zeyu Zhu[1†], Yining Zhu[2], Hao Luo[2], Yusi Wang[2], Yujie Liu[2], Hailan Wang[2], Wenjia Yuan[2], Yueguang Zhang[2], Chenying Yang[1,2*] and Weidong Shen[2*]

†Junren Wen, Xiao Chen and Zeyu Zhu contributed equally to this work.

*Correspondence:
ycheny@zju.edu.cn;
adongszju@hotmail.com

[1] Hangzhou Institute for Advanced Study, University of Chinese Academy of Sciences, Hangzhou 310024, China
[2] State Key Laboratory of Modern Optical Instrumentation, Department of Optical Engineering, Zhejiang University, Hangzhou 310027, China

Abstract

Colorful radiative coolers (CRCs) can be widely applied for energy sustainability especially and meet aesthetic purposes simultaneously. Here, we propose a high-efficiency CRC based on thin film stacks and engineered diffuse reflection unit, which brings out 7.1 °C temperature difference compared with ambient under ~ 700 W·m^{-2} solar irradiation. Different from analogous schemes, the proposed CRCs produce vivid colors by diffuse reflection and rest of the incident light is specular-reflected without being absorbed. Adopting the structure of TiO_2/SiO_2 multilayer stack, the nanophotonic radiative cooler shows extra low absorption across the solar radiation waveband. Significant radiative cooling performance can be achieved with the emissivity reaching 95.6% in the atmosphere transparent window (8–13 μm). Moreover, such CRC can be fabricated on flexible substrates, facilitating various applications such as the thermal management of cars or wearables. In conclusion, this work demonstrates a new approach for color display with negligible solar radiation absorption and paves the way for prominent radiative cooling.

Keywords: Radiative cooling, Color filter, Thin film, Energy sustainability

Introduction

As one of the most common passive devices in the field of optical films, color filters can be used in a wide range of application scenarios such as sensing, imaging, communication and architectural decoration. However, almost all kinds of color filters may face a common shortcoming, as they cannot withstand the strong radiation especially when placed outdoor. The reason is that the transmitted light will inevitably be absorbed by the absorbing materials, and the long-term strong solar radiation could possibly result in "thermal breakdown".

Cooling is one of the solutions to the problem we are facing, including active cooling and passive cooling methods. The former scheme such as air conditioning or water cooling requires additional energy consumption, and the loss weights the gain occasionally. Compared with active cooling, the environmental-friendly cooling method, passive cooling, does not consume energy by radiating the heat itself. Radiative cooling, an efficient and widely investigated approach to realize passive cooling, brings the energy of the object by radiation to the vast universe and achieve heat exchange [1–31]. The universe

is an ideal cooling source with the ultra-low temperature of 3K. However, the earth is surrounded by the atmosphere which serves as the "barrier" to protect our planet, allowing thermal emission at certain wavelengths to be transited. These wavelength ranges, where the atmosphere maintains high transmission, are known as the atmospheric windows. According to Wien's displacement law, the peak emission wavelength of an object at the room temperature (300K) locates at about 9 μm, so the atmosphere transparent window at 8–13 μm is highly concerned in terms of passive radiative cooling.

Recent years, combining of radiative cooling and color filters have become a hot research topic which can achieve energy sustainability as well as aesthetic purposes, and the CRCs can be employed as roofing materials and vehicle coatings [3, 12, 15, 16, 19–22, 25–31]. The main strategies include integration of radiative cooling materials with existing colorants and structural color filters [32]. For the latter, colors of the radiative coolers are nanostructure-induced and the mechanism for color display is totally different from the former. However, inevitable absorption of solar radiation will always occur though researchers have made great effect to narrow the absorption band in the solar wavelength range [3, 11, 12, 20, 21]. The average absorptions of the colorful passive thin film/opal-based radiative coolers are 40.0% at 0.3–1.8 μm [11], 16.7%/16.3%/10.7% for the samples in cyan/magenta/yellow colors within 0.3–0.8 μm [20], and 10.8%/12.3%/10.2% for the red/green/blue opals within 430-900 nm [21], respectively. The ratios mentioned above all exceed 10%, resulting in unavoidable temperature increment and affected efficiency for radiative cooling.

In this paper, we propose an efficient radiative cooler with specific diffuse reflection colors based on thin film structure and engineered diffuse reflection unit. Rather than conventional schemes that concentrate on narrowing the bandwidth of optical absorption, the proposed thin film-based colorful radiative cooler (CRC) reflected most of the solar radiation by both diffuse and specular reflection, and the final color is determined by the diffuse color mainly. The total reflection at 300-2500 nm is 95.8% which refers to an ultra-low absorption of the solar radiation. Two glass substrates are adopted in the proposed structure where the upper ZnS and TiO_2/SiO_2 stack are deposited on the smooth surface of the first substrate, and the Ag mirror is evaporated on the second smooth substrate. The back surface of the first substrate is rough and the two glass substrates are edge glued. High average emissivity (95.6%) over the atmosphere transparency window (8–13 μm) as well as vivid colors can be realized with the engineered thin film stack. Such structure can also be fabricated on flexible substrates and the application scenes can be furthered broadened. The proposed CRC represents a pioneering endeavor in the fabrication of highly efficient radiative cooling devices by harnessing the principles of diffuse light reflection for color display. This innovative approach offers new prospects for achieving enhanced cooling performance while simultaneously enabling vibrant and diverse color representations.

Results and discussion

The schematic of Film on Smooth surface-Mirror on Smooth surface (FS-MS) structure and the ideal specular/diffuse reflection are shown in Fig. 1(a-c). Theoretically, FS-MS can bring about nearly 100% specular reflection as well as 0% diffuse reflection in visible range, owing to high reflection of the metallic mirror on the smooth surface and low extinction coefficient of the thin film stack. However, such structure
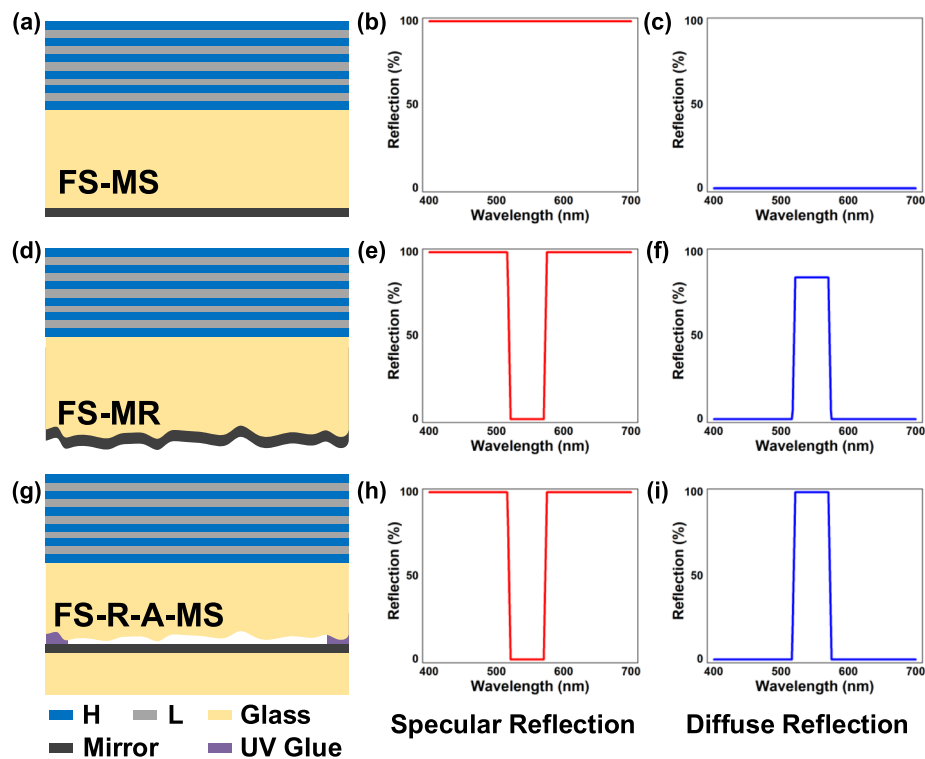
Fig. 1 a Structure of Film Stack-Mirror on Smooth surface (FS-MS). **b** Specular reflection of FS-MS in the visible wavelength range. **c** Diffuse reflection of FS-MS in the visible wavelength range. **d** Structure of Film Stack-Mirror on Rough surface (FS-MR). **e** Specular reflection of FS-MR in the visible wavelength range. **f** Diffuse reflection of FS-MR in the visible wavelength range. **g** Structure of Film Stack-Rough surface-Air-Mirror on Smooth surface (FS-R-A-MS). **h** Specular reflection of FS-R-A-MS in the visible wavelength range. **i** Diffuse reflection of FS-R-A-MS in the visible wavelength range

works like a "mirror" and does not own the function of color display. By replacing the back smooth surface of the substrate into a rough one, the total structure, Film on Smooth surface-Mirror on Rough surface (FS-MR), can generate zero specular reflection (100% direct transmission) in certain wavelength range by engineered color filters on the front smooth surface, shown in Fig. 1(d-e). Correspondingly, high diffuse reflection within the identical wavelength range can be realized, which is shown in Fig. 1(f). In this case, metal like silver (Ag) is deposited directly on the rough back surface, shown in Fig. S1, Supporting Information, and numerous micrometer or nanometer-scale surface irregularities or particles exist which can support the excitation of surface plasmon resonance (SPR) for electromagnetic waves, enhancing the light absorption on the metal/glass surface. The total reflection is reduced with the significant absorption caused by SPR effect, shown in Fig. S2, Supporting Information. Therefore, absorption of FS-MR in the visible range is unavoidable.

To lower the absorption within the solar irradiance waveband and ensure highly efficient radiative cooling, we proposed a brand-new structure, Film on Smooth surface-Rough surface-Air-Mirror on Smooth surface (FS-R-A-MS), and the schematic of the structure is shown in Fig. 1(g). The ideal specular and diffuse reflection of the proposed structure are shown in Fig. 1(h-i), where the diffuse reflection/color

is complementary to the specular reflection/color. Rather than depositing metallic film on the rough back surface of the first substrate shown in Fig. 1(d), the metallic mirror here is deposited on another transparent substrate with a smooth surface, and two substrates are edge glued by UV glue. The rough surface, the metallic mirror, and the air cavity compose the diffuse reflection unit. Such modified diffuse reflection unit can avoid the micro-nano structure along with SPR and effectively mitigates the unnecessary absorption of solar radiation. To investigate the structure influence of the diffuse reflection unit, we conduct an in-depth analysis of the thickness of the air cavity and the roughness of the rugged surface with FDTD Solutions (The configuration of the diffuse reflection unit for simulation is shown in Fig. S3, Supporting Information). In our work, Ag is used as the mirror material. It is confirmed that both parameters have little influence on the overall high reflection of the structure for the visible-near infrared band, which can be observed in Fig. S4, Supporting Information. The high reflection (~99%) can be obtained for different thicknesses of the air cavity, ranging from 1 μm to 100 μm, and the high reflection (~99%) can also be maintained for different roughnesses. So, the thickness of the air cavity and roughness of the rough surface can be chosen from a wide range for FS-R-A-MS. Moreover, the comparison between the diffuse reflection units applied in FS-MR and FS-R-A-MS can be visually illustrated through the simulated reflection/absorption spectra, as shown in Fig. S5, Supporting Information.

Adopting the structure in Fig. 1(g), we try to realize the function of radiative cooling as well as color display concurrently. The complete structure of the proposed CRC contains the top anti-reflection layer, a high-emissivity color filter, a visible-transparent substrate and a diffuse reflection unit. With distinct parameters of the color filter (TiO$_2$/SiO$_2$ film stack typically), e.g. different layer numbers and thickness of each layer, the proposed structure can reveal vivid colors, shown in Fig. 2(a). Tables S1, S2, S3, S4, S5 and S6 present the optimized layer numbers and thicknesses of each layer constituting the film stacks. The number of layers in all samples are limited to ensure feasible industrial manufacturing, and the total thickness of the film stack is less than 2.5 μm. The designed/measured specular reflection, and the measured diffuse reflection of Sample #5 at the wavelength range of 400–700 nm are shown in Fig. 2(b), where the measured specular/diffuse reflection of the rest samples are shown in Fig. S6, Supporting Information. Moreover, by fixing the incidence angle of the illuminated light source to 10° (The experimental setup is shown in Fig. S7, Supporting Information), angle-resolved reflection spectra of all samples and the corresponding colors are displayed in Figs. S8 and S9, Supporting Information. By analyzing reflection and the final color of all samples, we can find that the diffuse reflection spectrum mainly determines the final color of the sample at most viewing angles. The reason is that the incident light is typically highly divergent in practical viewing scenarios, and as such, the final color of the proposed CRC is governed by the dominant intensity in the spatial domain, specifically the diffuse color. Stated differently, considering a point on the CRC, only one beam of light corresponds to specular reflection, while the others are diffuse reflected lights. Figure 2(c) displays digital photographs of Sample #4 captured from viewing angles ranging from 0° to 55°, demonstrating that the proposed CRC exhibits advantageous angle-independence within ±50° viewing angles. The total reflection of Sample #5 in ultraviolet–visible-near infrared is shown in Fig. 2(d),
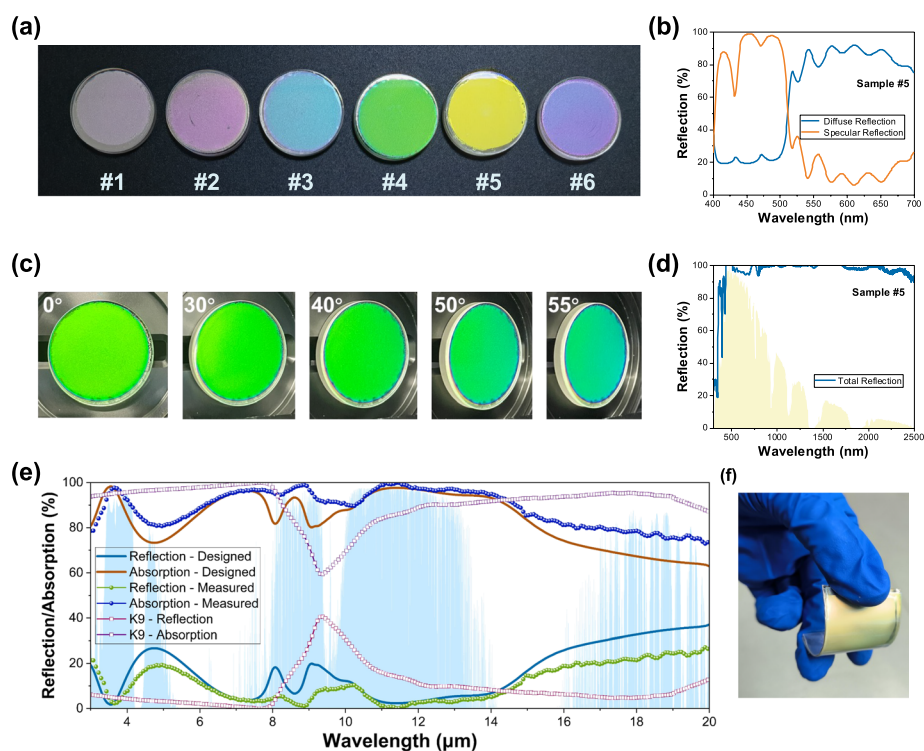
Fig. 2 Appearance and optical characteristics of the proposed thin film-based CRC. **a** Appearance of the CRCs. The color filters on the first BK7 glass substrates are optimized to exhibit distinct colors. **b** Measured specular/diffuse reflection of Sample #5 in the wavelength range of 400–700 nm. **c** Digital photographs of Sample #4 captured from viewing angles ranging from 0° to 55°, and the proposed CRC exhibits outstanding angle-independence within ± 50° viewing angles. **d** Total reflection of Sample #5 in ultraviolet–visible-near infrared range (300–2500 nm). The AM1.5 solar spectrum (the light yellow area) is plotted for reference. **e** The reflection/absorption of the bare BK7 glass substrate and the designed/measured reflection/absorption of the proposed CRC in the wavelength range of 3–20 μm. The atmosphere transparency window (the light blue area) is plotted as reference. **f** The proposed CRC fabricated on a flexible PC substrate

and ultra-high reflection (95.8%) can be obtained within 300–2500 nm. The exceptionally high reflectance can be attributed to the underlying factors. By utilizing thin film materials with ultra-low extinction coefficient in the visible-infrared region, the incident light is predominantly either transmitted or specular-reflected without significant absorption. Additionally, modifying the back surface of the first substrate to introduce a rough texture, coupled with a high-reflection mirror beneath, almost all the transmitted light (up to 99%) is diffuse-reflected back into the incident medium. We further conduct a comprehensive analysis to investigate the potential influence of the geometric characteristics of the randomly textured surface on the coloration performance. Adopting the identical experimental setup depicted in Fig. S7, Supporting Information, angle-resolved reflection spectra of Sample #5 with distinct levels of roughness are measured and compared. The top BK7 glass substrates adopted in the proposed CRC are prepared by grinding using 280#, 600#, and 1000# emery particles respectively, and the microscope image of the samples are shown in Figure S10, Supporting Information. The measured reflection spectra are shown in Figures S11, S12 and S13, Supporting Information. By comparing the specular reflection spectra at the reflected angle of 10°, shown in Figure S12, Supporting Information, we observe that the reflections of the samples are nearly identical and

remain unaffected by the introduction of the rough surface. And the slight variations are attributed to the inevitable difference in film thickness, due to the varying positions of the substrates in the chamber during deposition. However, the intensities of the diffuse reflected light varied for different roughnesses, as shown in Figure S13, Supporting Information. By using denser emery particles, the specular reflected light is more concentrated due to weaker scattering, thereby achieving a more localized distribution of light intensity. Therefore, the proposed CRC employs a brand-new method for color display and achieves a remarkably low level of solar radiation absorption, creating a proper objective condition for exquisite radiative cooling performance.

To achieve prominent radiative cooling performance, high mid-infrared emissivity covering the atmosphere transparency window of 8–13 μm is required for a practical CRC. The visible-transparent substrate adopted in the proposed CRC is the BK7 glass and the reflection/absorption spectra at 3–20 μm are shown in Fig. 2(e). The BK7 glass shows an overall high absorption (80.7%) at 8–13 μm, but an absorption dip at around 8.5–10.5 μm exists because of a large impedance mismatch between the bare BK7 glass and the air. With the help of the top anti-reflection layer and the radiative cooling color filter, the absorption of FS-R-A-MS are enhanced compared with base BK7 glass, especially at 8.5–10.5 μm. Specifically, SiO_2 layers maintains high absorption at 8–10 μm while TiO_2 shows high absorption at 10–14 μm, so the proposed CRC reveals high absorption among the atmosphere transparency window [8]. As a result, the average designed/measured absorption of FS-R-A-MS device at 8–13 μm are 92.1% and 95.6% respectively, and the designed/measured absorption and reflection spectra at the wavelength range of 3–20 μm are shown in Fig. 2(e). Moreover, the BK7 glass substrates in FS-R-A-MS can be replaced by flexible flat ones such as PC and PET, shown in Fig. 2(f), indicating broadened application occasions, e.g. wearable devices, where the colorful radiative coolers should be curable or flexible. Since the second substrate is not involved in radiative cooling, it can be replaced with any substrate that can be easily coated with the Ag mirror.

Furthermore, the crucial film stack including the upper anti-reflection layer and the dielectric constitution is intensively analyzed on the effect of both color display and radiative cooling. To further enlarge the absorption in the atmosphere transparency window, ZnS is added on the top of the dielectric film stack as the anti-reflection layer and helps to achieve lower reflection in mid to far-infrared, thus advanced cooling performance [33]. Color display and extremely low absorption in visible-near infrared will not be affected by introducing ZnS, owing to its low extinction coefficients in the visible-near infrared wavelength range. The reflection/absorption of FS-R-A-MS at 8–13 μm with/without ZnS is depicted in Fig. 3(a). It can be observed that the employment of upper ZnS layer leads to a lower average reflection, resulting in a larger average emissivity of the overall structure within the atmosphere transparency window. The average absorption with/without ZnS are 92.0% and 89.0% respectively. In another aspect, the materials of the color filter will significantly influence the characteristics of the proposed CRC, and we systematically study distinct thin film stacks serving as the color filters. The thicknesses of the film layers are optimized to exhibit the same color, and the parameters are shown in Tables S5, S7 and S8, Supporting Information for TiO_2/SiO_2, TiO_2/Al_2O_3, and Al_2O_3/SiO_2 stacks, respectively. TiO_2/SiO_2 and Al_2O_3/SiO_2 stacks can offer lower
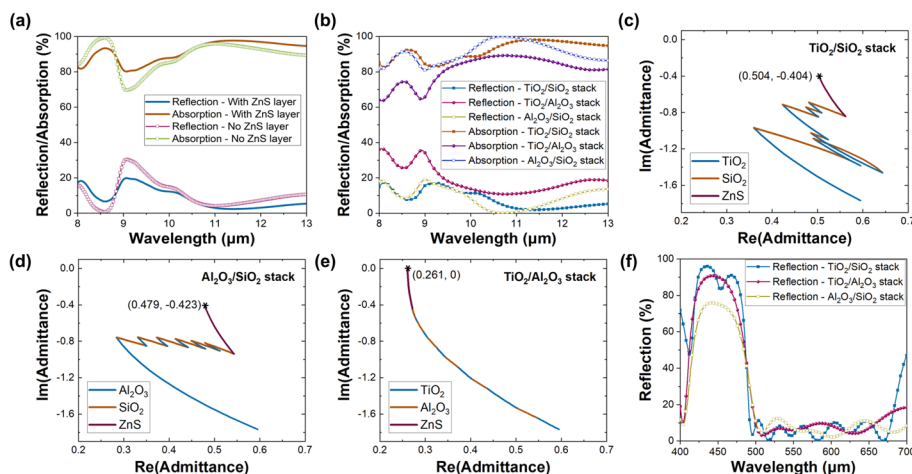
Fig. 3 a Reflection/absorption of FS-R-A-MS with/without upper ZnS in 8–13 μm. **b** Reflection/absorption of FS-R-A-MS at 8–13 μm, which use TiO_2/SiO_2, Al_2O_3/SiO_2 and TiO_2/Al_2O_3 stack as the color filter. **c** Optical admittance locus of TiO_2/SiO_2 stack with the upper ZnS. **d** Optical admittance locus of Al_2O_3/SiO_2 stack with the upper ZnS. (**e**) Optical admittance locus of TiO_2/Al_2O_3 stack with the upper ZnS. **f** Reflection of TiO_2/SiO_2, Al_2O_3/SiO_2 and TiO_2/Al_2O_3 stack at 400–700 nm

reflection thus higher absorption compared with TiO_2/Al_2O_3 stack across 8–13 μm wavelengths, especially at 8.5–9.5 μm, shown in Fig. 3(b). According to the proposed CRC, no light will pass through the whole structure due to the bottom mirror, therefore the high absorption corresponds to the low reflection, which can be investigated by the optical admittance (inverse of the impedance) for those unmatched-index wavelengths, and Fig. 3(c-e) reveal the optical admittance loci of the three multilayer film stacks of the color filter with the upper ZnS at 9 μm. We can easily find that the admittance of TiO_2/SiO_2 and Al_2O_3/SiO_2 stack approach (1, 0), the index of the incident medium (air), spirally. The low reflection of the structure characterized by the length between the final admittance and the air's admittance is verified here. The extinction coefficient of SiO_2 at 9 μm is much higher than the value in visible-near infrared range, and SiO_2 shows the optical characteristic similar to metal, while the extinction coefficient of the adopted TiO_2 and Al_2O_3 are close to zero, indicating the feature of dielectric layers. By combing a metal-like and a dielectric-like material, the admittance of the films on the first substrate becomes small and matches that of the air, which ensures a low Fresnel reflection [34–38]. On the other hand, by adopting TiO_2/Al_2O_3 stack, the admittance varied in one direction owing to the low extinction coefficient of both materials, so the admittance remains big and the reflection at the corresponding wavelength is much higher than the other two film stacks. However, considering the reflection in visible range, TiO_2/SiO_2 stack provides higher specular reflection than Al_2O_3/SiO_2 stack in 400–500 nm, shown in Fig. 3(f), which refers to an advanced manifestation of the desired color. The same results can be attained for other colors, as illustrate in Fig. S14, Supporting Information. Based on the comparison above, we choose the preferred TiO_2/SiO_2 stack as the color filter in our proposed colorful radiative cooler. But the available material combination for the color filter is not limited. The reflection/absorption within the atmosphere transparency window and the reflection in the visible range of Ta_2O_5/SiO_2 stack are shown in
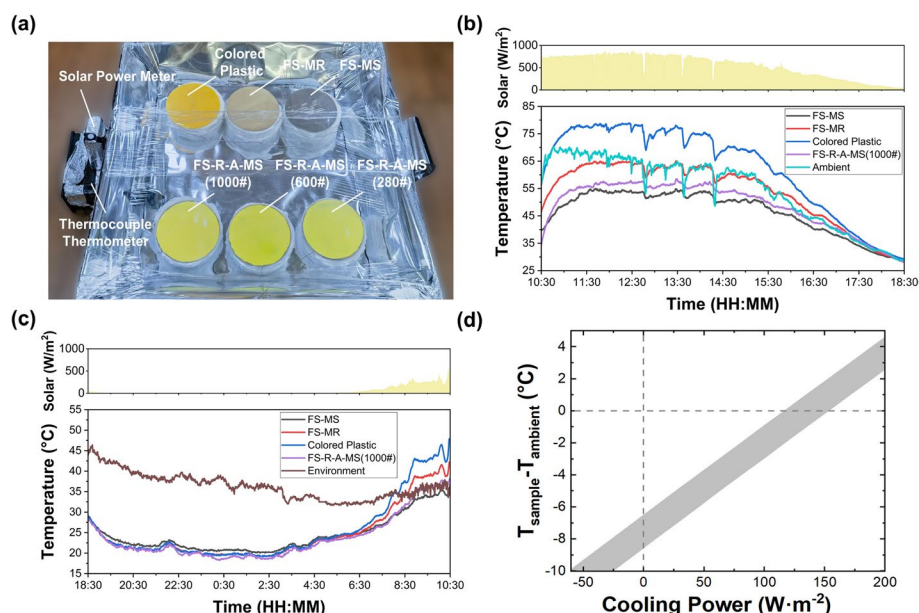
Fig. 4 Radiative cooling performance of the proposed CRC. **a** Schematic diagram of the testing equipment for experimentally evaluating the radiative cooling ability. **b** The temperature variation of FS-MS, FS-MR, colored plastic, FS-R-A-MS (1000#, 680#, and 280#) and ambient during the testing hours between 10:30 and 18:30. The solar irradiation (the light yellow area) is plotted for reference, and the average radiance between 11:30 and 15:30 is ~700W·m^{-2}. **c** The temperature variation of FS-MS, FS-MR, colored plastic, FS-R-A-MS (1000#, 680#, and 280#) and environment during the testing hours between 18:30 and 10:30 (the next day). The solar irradiation (the light yellow area) is plotted for reference. **d** Estimated cooling power of the proposed CRC. The value of non-radiative heat coefficient (h$_c$) is 13 W·m^{-2}·K^{-1} by linear regression, and the solar irradiance is set as 850 W·m^{-2}

Fig. S15, Supporting Information. Due to similar optical constants of Ta$_2$O$_5$ and TiO$_2$, Ta$_2$O$_5$/SiO$_2$ stack provides analogous level of absorption in 8–13 μm (~92.2%) and similar purity of the color comparable with the adopted TiO$_2$/SiO$_2$ stack.

We experimentally evaluate the radiative cooling ability of the proposed CRC in Xihu District, Hangzhou, China (30°16'N, 120°12'E). The schematic diagram of the testing equipment is shown in Fig. 4 (a) (see Methods section for further details). The thermocouple thermometer is employed to gauge the temperatures of the samples, while a solar power meter is utilized to quantify the real-time intensity of solar radiation. We record the real-time temperatures of the samples (FS-MS, FS-MR, colored plastic and FS-R-A-MS with varying roughnesses) throughout the entire day, with the thermocouples securely affixed to the rear of the samples. As is shown in Fig. S16, Supporting Information, the average temperatures of FS-R-A-MS, featuring roughness parameters of 1000#, 600#, and 280#, are recorded as 32.2 °C, 32.7 °C, and 33.0 °C, respectively. Based on the observations, we infer that the level of roughness in the diffuse reflection unit exerts low influence on the cooling performance, which aligns with the aforementioned optical characteristics. We further analyze the cooling performance between the hours of 11:30 and 15:30, with the solar irradiation of ~700W·m^{-2} during the procedure. As is depicted in Fig. 4(c), FS-MS (the black line) and colored plastic (the blue line) show the lowest and highest temperature respectively. In this circumstance, FS-MS acts as a "mirror" and the total reflection is the highest among all samples. FS-MR (the red line) shows evident cooling effect compared

with the colored plastic, and the average temperature decrement is 11.9 °C within the testing procedure. The proposed colorful radiative cooler, FS-R-A-MS (the red line) reflects markedly advanced cooling than FS-MR owing to the improved diffuse reflection module. The average temperature difference between FS-R-A-MS and FS-MR/colored plastic is 6.5 °C/18.4 °C, which origins mainly from the deceased absorption of solar radiation. In a remarkable feat, our study further reveals that FS-R-A-MS can achieve cooling temperatures below ambient levels, recording a substantial average value of 7.1 °C. This noteworthy capability reinforces the potential of the proposed CRC in contributing to advances in the field of colorful radiative cooling. We compare the temperatures of samples with the environment at night, depicted in Fig. 4(d). Between the hours of 18:30 and 6:30 (the next day), the average temperature decrement of FS-R-A-MS and environment is 15.9 °C. Moreover, cooling power of the proposed CRC is estimated, and the approach used to establish this model adheres to the methodology delineated in Ref. [4]. By linear regression, the value of non-radiative heat coefficient (h_c) is 13 W·m^{-2}·K^{-1}, and the solar irradiance is set as 850 W·m^{-2}. The cooling power is 116.1–153.0 W·m^{-2} considering the uncertainty of the atmospheric transmittance. Also, the steady-state temperature decrement of 6.5–8.6 °C below ambient levels can be achieved for the proposed CRC, and the similative result is in accordance with the experimental one. The performance metric further accentuates the efficacy of the CRC in the realm of passive cooling applications.

As is experimentally depicted above, temperature decrement is closely related to the absorption at ultraviolet–visible-near infrared wavelengths, and thus we simulatively quantify the correlation. The emission in the atmosphere transparent window *e* is assumed 100%, and the correlation between temperature (°C) and solar irradiation (W·m^{-2}) of the three samples whose absorption of the solar radiation *a* are 0, 0.05 and 0.1 are compared, illustrated in Fig. S17, Supporting Information. Under 850 W·m^{-2} solar irradiation, the temperatures of the three samples are -2.58 °C, 4.23 °C and 10.93 °C, respectively, when the ambient temperature is set as 20 °C. We can conclude that unnecessary absorption of solar radiation will result in temperature increment of the samples, thus make significant impact on the cooling performance, which validates the experimental results of different samples.

Conclusion

In summary, we propose a colorful radiative cooler (CRC) based on thin film stacks which can be widely used for thermal management and energy sustainability. The basic structure, Film on smooth surface-Rough surface-Air-Metal on smooth surface (FS-R-A-MS), consists of the upper ZnS film, TiO$_2$/SiO$_2$ stack, the first BK7 glass substrate (the front surface is smooth, and the back surface is rough), Ag mirror and the second BK7 glass substrate (both surfaces are smooth). With this structure, ultra-low (4.2%) absorption of the solar radiation within 300–2500 nm can be achieved, bringing outstanding objective conditions for radiative cooling. Moreover, the proposed CRC shows high emissivity within the atmosphere transparent window, and the average designed/measured absorption in 8–13 µm are 92.1% and 95.6% respectively. Also, we prove the significant cooling performance of the proposed CRC experimentally. The average temperature decrements between the proposed colorful radiative cooler and ambient/FS-MR/colored plastic are 7.1 °C/6.5 °C/18.4 °C, respectively. Different from previous works which

concentrate on narrowing the optical absorption bandwidth, the proposed CRC utilizes a diffuse reflection module for color display and ensures ultra-low absorption of solar radiation by engineered thin film stack, demonstrating effective color display as well as exceptional radiative cooling performance both theoretically and experimentally.

Methods

Preparation of samples

The top ZnS and TiO_2/SiO_2 stack of FS-MS, FS-MR and FS-R-A-MS on the BK7 glass substrates were fabricated by thermal evaporation with the deposition rate of 0.3 nm/s, 0.3 nm/s and 0.6 nm/s for ZnS, TiO_2 and SiO_2 respectively. The optical constants of the deposited materials (TiO_2, SiO_2, and ZnS) within visible-near infrared region were determined by spectrometry method using optiLayer, taking into account the reflectance and transmittance curves. The optical constants of each material are presented in Figure S18, Supporting Information. To achieve the rugged surfaces with varying roughnesses, the BK7 glass substrates were realized by grinding using 1000#, 600#, and 280# emery particles respectively. The Ag films on the smooth/rough surfaces were deposited by thermal evaporation with a vacuum pressure less than 2×10^{-3} Pa at room temperature. Finally, the color filtering substrate with a smooth bottom surface and the diffuse reflection module with the Ag mirror on the rough surface were edge glued by UV glue, constructing the proposed FS-R-A-MS device.

Spectra characterization for samples

The specular reflection spectra, angle-resolved reflection spectra of the samples were measured by the commercial spectrometer Cary 7000 with angle-resolved UMA from Agilent Technologies Inc and Hitachi UH4150 with angle-resolved reflection/transmission accessory. Total reflection and diffuse reflection were measured by Cary 7000 spectrometer with the integrating sphere in different settings, respectively. The reflection/transmission of the fabricated samples for middle and far infrared band (2.5–20 μm) was performed using the Fourier transform infrared spectroscopy Vertex 70 from Bruker Inc.

Testing equipment for evaluating the radiative cooling ability

The testing equipment was 50×50 cm^2, and the material of the equipment was EPS foam. The six samples with diameter of 120 mm each, colored plastic, FS-MS, FS-MR and FS-R-A-MS (1000#, 600#, and 280#), were placed on the aerogel to avoid heat delivering to the equipment. The undersurface was covered by aluminum foil to reflect solar irradiation and the entire equipment was sealed with the PE film on top of the air chamber. The thermocouple under each sample measured the temperature, and the solar power meter was used to define the intensity of solar radiation in real time. The ambient temperature is measured using thermocouple in the shelter placed in the testing equipment, and the environment temperature is also measured using thermocouple in the shelter placed out of the testing equipment.

Abbreviations
CRC   Colorful radiative cooler

SPR   Surface Plasmon Resonance
FS-MS   Film stack on Smooth surface-Mirror on Smooth surface
FS-MR   Film stack on Smooth surface-Mirror on Rough surface
FS-R-A-MS   Film stack on Smooth surface-Rough surface-Air-Mirror on Smooth surface

Supplementary Information

The online version contains supplementary material available at https://doi.org/10.1186/s43074-023-00104-5.

Additional file 1: Fig. S1. The SEM cross-section image of the Ag mirror on the rough surface. **Fig. S2.** Total reflection/absorption of the Ag mirror on rough surface in the wavelength range of 400-2500nm. **Fig. S3.** The configuration of the diffuse reflection unit for simulation. The morphology of the rugged surface is based on the data collected by the step profiler. The purple arrow denotes the direction of the incident light. (a-b) The diffuse reflection unit applied in FS-R-A-MS with different rough surfaces. The rugged surface is prepared by using 280# and 1000# emery particles, respectively, and Ag (the thin layer in blue) is coated on the smooth surface of the bottom BK7 glass substrate. As an example, the air cavity is set to a thickness of 10 μm. (c-d) The diffuse reflection unit applied in FS-MR with different rough surfaces. The rugged surface is prepared by using 280# and 1000# emery particles, respectively, and Ag film (the thin layer in blue color) is directly coated on the rugged surface. **Fig. S4.** Simulation analysis of the thickness of the air cavity and the roughness of the rugged surface on the optical characteristics. (a-c) Total reflection and absorption of FS-R-A-MS with rugged surface prepared by using 280# emery particles. The thicknesses of the air cavity is set as 1 μm, 10 μm and 100 μm, respectively. (d-f) Total reflection and absorption of FS-R-A-MS with rugged surface prepared by using 1000# emery particles. The thicknesses of the air cavity is set as 1 μm, 10 μm and 100 μm, respectively. **Fig. S5.** Comparison between the diffuse reflection units applied in FS-MR and FS-R-A-MS on the optical characteristics. (a-b) Total reflection and absorption of FS-MR with rugged surface prepared by using 280# and 1000# emery particles, and Ag film is directly coated on the rugged surface. (c-d) Total reflection and absorption of FS-MR with rugged surface prepared by using 280# and 1000# emery particles, and Ag film is coated on the smooth surface of the bottom BK7 glass substrate. **Fig. S6.** The measured specular/diffuse reflection of Sample #1, Sample #2, Sample #3, Sample #4 and Sample #6 in Fig. 2(a). **Fig. S7.** Experimental setup for measuring the angle-resolved reflection spectra. The incidence angle of the illuminated light source is fixed to 10° (the orange line), and the specular reflected light is observed within reflected angles ranging from 0° to 60°. Specially, the specular reflected light can only be observed at a narrow reflected angle range centered at 10° (the red line). **Fig. S8.** Angle-resolved reflection spectra measured by spectrophotometer and diffuse colors of all samples marked in CIE 1931 chromatic diagram. (a-f) Angle-resolved specular reflection spectra of Sample #1 to #6. The incidence angle of the illuminated light source is fixed to 10°, and the specular reflected light is dominant at the reflected angles of 5° and 10°. (g-i) Angle-resolved diffuse reflection spectra of Sample #1 to #6. The incidence angle of the illuminated light source is fixed to 10°, and the diffuse reflected light can be observed at reflected angles of 0°, 15°, 20°, 25°, 30°, 35°, 40°, 45°, 50°, 55° and 60°. The intensity of the diffuse reflected lights are much lower than the specular reflected ones under this circumstance, because the illuminated light is highly collimated in the spectrophotometer. (m-r) Chromaticity coordinates of the Diffuse colors are calculated and marked in CIE 1931 chromatic diagrams. **Fig. S9.** Angle-resolved specular/diffuse reflection spectra of Sample #5. The incidence angle of the illuminated light source is fixed to 10°, and the specular reflected light can only be observed at a narrow reflected angle range of 5°- 13°. **Fig. S10.** (a-c) Microscope images (scale bars, 100 μm) of the rough surfaces adopted in FS-R-A-MS with varying levels of roughness. The rough surfaces were prepared by grinding using 280#, 600#, and 1000# emery particles respectively. **Fig. S11.** Angle-resolved specular/diffuse reflection spectra of samples with distinct levels of roughness. The parameters of the upper anti-reflection layer and the color filter are identical for all samples. The experimental setup is shown in Fig. S4, Supporting Information, with the incidence angle of the illuminated light source fixed to 10°. (a-c) Angle-resolved specular reflection spectra of samples with rough surfaces prepared by 280#, 600# and 1000# emery particles respectively. The specular reflected light can only be observed at reflected angles of 5° and 10°. (d-f) Angle-resolved diffuse reflection spectra of samples with rough surfaces prepared by 280#, 600# and 1000# emery particles respectively. The incidence angle of the illuminated light source is fixed to 10°, and the diffuse reflected light is collected at reflected angles of 0°, 15°, 20°, 25°, 30°, 35°, 40°, 45°, 50°, 55° and 60°. **Fig. S12.** Specular reflection spectra of samples with distinct levels of roughness. The parameters of the upper anti-reflection layer and the color filter are identical for all samples, and the rough surfaces are prepared by 280#, 600# and 1000# emery particles respectively. **Fig. S13.** Diffuse reflection spectra of samples with distinct levels of roughness. The parameters of the upper anti-reflection layer and the color filter are identical for all samples, and the rough surfaces are prepared by 280#, 600# and 1000# emery particles respectively. (a) Diffuse reflection spectra observed at a reflected angle of 15°. (b) Diffuse reflection spectra observed at a reflected angle of 60°. **Fig. S14.** (a) Reflection of TiO_2/SiO_2, Al_2O_3/SiO_2 and TiO_2/Al_2O_3 stacks at 400-700 nm for Sample #4. (b-d) Optical admittance loci of TiO_2/SiO_2, Al_2O_3/SiO_2 and TiO_2/Al_2O_3 stacks with the upper ZnS for Sample #4. (e) Reflection of TiO_2/SiO_2, Al_2O_3/SiO_2 and TiO_2/Al_2O_3 stacks at 400-700 nm for Sample #6. (f-h) Optical admittance loci of TiO_2/SiO_2, Al_2O_3/SiO_2 and TiO_2/Al_2O_3 stacks with the upper ZnS for Sample #6. **Fig. S15.** (a) Reflection/absorption of FS-R-A-MS with Ta_2O_5/SiO_2 stack in 8-13 μm. (b) Reflection of FS-R-A-MS with Ta_2O_5/SiO_2 stack in 400-700nm. **Fig. S16.** The temperature variation of FS-R-A-MS (1000#, 680#, and 280#) and colored plastic throughout the entire day. **Fig. S17.** Correlation of solar irradiation and temperature within three samples which own different absorptions ***a*** and an ideal emission ***e***. The ambient temperature is set as 20°C. **Fig. S18.** The optical constants of TiO_2, SiO_2 and ZnS within 0.38-20 μm range. **Table S1.** Table of Thin Film Layer Thickness and Materials for Sample #1. **Table S2.** Table of Thin Film Layer Thickness and Materials for Sample #2. **Table S3.** Table of Thin Film Layer Thickness and Materials for Sample #3. **Table S4.** Table of Thin Film Layer Thickness and Materials for Sample #4. **Table S5.** Table of Thin Film Layer Thickness and Materials for Sample #5. **Table S6.** Table of Thin Film Layer Thickness and Materials for Sample #6. **Table S7.** Table of Thin Film Layer Thickness and Materials for TiO_2/Al_2O_3 Stack. **Table S8.** Table of Thin Film Layer Thickness and Materials for Al_2O_3/SiO_2 Stack.

Declarations

Ethics approval and consent to participate
Not applicable.

Consent for publication
Not applicable.

Competing interests
The authors declare that they have no competing interests.

References

1. Harrison AW, Walton MR. Radiative cooling of TiO_2 white paint. Sol Energy. 1978;20(2):185–8.
2. Granqvist CG, Hjortsberg A. Surfaces for radiative cooling: silicon monoxide films on aluminum. Appl Phys Lett. 1980;36(2):139–41.
3. Zhu L, Raman A, Fan S. Color-preserving daytime radiative cooling. Appl Phys Lett. 2013;103:223902.
4. Raman AP, Anoma MA, Zhu L, Rephaeli E, Fan S. Passive radiative cooling below ambient air temperature under direct sunlight. Nature. 2014;515:540–4.
5. Chen Z, Zhu L, Raman A, Fan S. Radiative cooling to deep sub-freezing temperatures through a 24-h day–night cycle. Nat Commun. 2016;7:13729.
6. Hossain MM, Gu M. Radiative cooling: principles, progress, and potentials. Adv Sci. 2016;3(7):1500360.
7. Zhai Y, Ma Y, David SN, Zhao D, Lou R, Tan G, Yang R, Yin X. Scalable-manufactured randomized glass-polymer hybrid metamaterial for daytime radiative cooling. Science. 2017;355(6329):1062–6.
8. Ono M, Chen K, Li W, Fan S. Self-adaptive radiative cooling based on phase change materials. Opt Express. 2018;26(18):A777–87.
9. Sun K, Riede CA, Wang Y, Urbani A, Simeoni M, Mengali S, Zalkovskij M, Bilenberg B, de Groot CH, Muskens OL. Metasurface optical solar reflectors using AZO transparent conducting oxides for radiative cooling of spacecraft. ACS Photonics. 2018;5(2):495–501.
10. Yuan H, Yang C, Zheng X, Mu W, Wang Z, Yuan W, Zhang Y, Chen C, Liu X, Shen W. Effective, angle-independent radiative cooler based on one-dimensional photonic crystal. Opt Express. 2018;26(21):27885–93.
11. Li W, Shi Y, Chen Z, Fan S. Photonic thermal management of coloured objects. Nat Commun. 2018;9:4240.
12. Lee G, Kim Y, Kim H, Yoo Y, Song Y. Colored, daytime radiative coolers with thin-film resonators for aesthetic purposes. Adv Opt Mater. 2018;6(22):1800707.
13. Zhao D, Aili A, Zhai Y, Xu S, Tan G, Yin X, Yang R. Radiative sky cooling: fundamental principles, materials, and applications. Appl Phys Rev. 2019;6:021306.
14. Zhao B, Hu M, Ao X, Chen N, Pei G. Radiative cooling: a review of fundamentals, materials, applications, and prospects. Appl Energy. 2019;236:489–513.
15. Sheng C, An Y, Du J, Li X. Colored radiative cooler under optical Tamm resonance. ACS Photonics. 2019;6(10):2545–52.
16. Lozano LM, Hong S, Huang Y, Zandavi H, El Aoud YA, Tsurimaki Y, Zhou J, Xu Y, Osgood RM, Chen G, Boriskina SV. Optical engineering of polymer materials and composites for simultaneous color and thermal management. Opt Mater Express. 2019;9(5):1990–2005.
17. Yin X, Yang R, Tan G, Fan S. Terrestrial radiative cooling: Using the cold universe as a renewable and sustainable energy source. Science. 2020;370(6518):786–91.
18. Li Z, Chen Q, Song Y, Zhu B, Zhu J. Fundamentals, materials, and applications for daytime radiative cooling. Adv Mater Technol. 2020;5(5):1901007.
19. Han RPS, Cao A, Yang Y. Colored and paintable bilayer coatings with high solar-infrared reflectance for efficient cooling. Sci Adv. 2020;6(17):eaaz5413.
20. Yalçın R, Blandre E, Joulain K, Drévillon J. Colored radiative cooling coatings with nanoparticles. ACS Photonics. 2020;7(5):1312–22.

21. Kim H, Im E, Lee S. Colloidal photonic assemblies for colorful radiative cooling. Langmuir. 2020;36(23):6589–96.
22. Chen Y, Mandal J, Li W, Smith-Washington A, Tsai CC, Huang W, Shrestha S, Yu N, Han RPS, Cao A, Yang Y. Colored and paintable bilayer coatings with high solar-infrared reflectance for efficient cooling. Sci Adv. 2020;6(17):eaaz5413.
23. Zeng S, Pian S, Su M, Wang Z, Wu M, Liu X, Chen M, Xiang Y, Wu J, Zhang M, Cen Q, Tang Y, Zhou X, Huang Z, Wang R, Tunuhe A, Sun X, Xia Z, Tian M, Chen M, Ma X, Yang L, Zhou J, Zhou H, Yang Q, Li X, Ma Y, Tao G. Hierarchical-morphology metafabric for scalable passive daytime radiative cooling. Science. 2021;373(6555):692–6.
24. Luo H, Zhu Y, Xu Z, Hong Y, Ghosh P, Kaur S, Wu M, Yang C, Qiu M, Li Q. Outdoor personal thermal management with simultaneous electricity generation. Nano Lett. 2021;21(9):3879–86.
25. Yoon TY, Son S, Min S, Chae D, Woo HY, Chae J, Lim H, Shin J, Paik T, Lee H. Colloidal deposition of colored daytime radiative cooling films using nanoparticle-based inks. Mater Today Phys. 2021;21:100510.
26. Zhu Y, Luo H, Yang C, Qin B, Ghosh P, Kaur S, Shen W, Qiu M, Belov P, Li Q. Color-preserving passive radiative cooling for an actively temperature-regulated enclosure. Light Sci Appl. 2022;11(1):1–9.
27. Yu S, Zhang Q, Wang Y, Lv Y, Ma R. Photonic-structure colored radiative coolers for daytime subambient cooling. Nano Lett. 2022;22(12):4925–32.
28. Chen Y, Mandal J, Li W, Smith-Washington A, Tsai CC, Huang W, Shrestha S, Yu N, Xu J, Wan R, Xu W, Ma Z, Cheng X, Yang R, Yin X. Colored radiative cooling coatings using phosphor dyes. Mater Today Nano. 2022;19:100239.
29. Zhu W, Droguet B, Shen Q, Zhang Y, Parton TG, Shan X, Parker RM, De Volder MFL, Deng T, Vignolini S, Li T. Structurally colored radiative cooling cellulosic films. Adv Sci. 2022;9(26):2202061.
30. Liu H, Kang H, Jia X, Qiao X, Qin W, Wu X. Commercial-like self-cleaning colored ZrO$_2$-based bilayer coating for remarkable daytime sub-ambient radiative cooling. Adv Mat Tec. 2022;7(10):2101583.
31. Guan Q, Raza A, Mao SS, Vega LF, Zhang T. Machine learning-enabled inverse design of radiative cooling film with on-demand transmissive color. ACS Photonics. 2023;10(3):715–26.
32. Zhou L, Rada J, Song H, Ooi B, Yu Z, Gan Q. Colorful surfaces for radiative cooling. J Photonics Energy. 2021;11(4):042107.
33. Yang C, Ji C, Shen W, Lee K-T, Zhang Y, Liu X, Guo LJ. Compact multilayer film structures for ultrabroadband, omnidirectional, and efficient absorption. ACS Photonics. 2016;3(4):590–6.
34. Yang C, Wen J, Chen X, Luo H, Zhu Y, Wang H, Zheng T, Zhang Y, Shen W. Wavelength-Selective light trapping with nanometer-thick metallic coating. Adv Photonics Res. 2022;3(7):2100338
35. Sergeant NP, Pincon O, Agrawal M, Peumans P. Design of wide-angle solar-selective absorbers using aperiodic metal-dielectric stacks. Opt Express. 2009;17(25):22800–12.
36. Zhu P, Guo LJ. High performance broadband absorber in the visible band by engineered dispersion and geometry of a metal-dielectric-metal stack. Appl Phys Lett. 2012;101(24):241116.
37. Chen F, Wang S, Liu X, Ji R, Yu L, Chen X, Lu W. High performance colored selective absorbers for architecturally integrated solar applications. J Mater Chem A. 2015;3(14):7353–60.
38. Ji C, Lee KT, Xu T, Zhou J, Park HJ, Guo LJ. Engineering light at the nanoscale: structural color filters and broadband perfect absorbers. Adv Opt Mater. 2017;5(20):1700368.

Publisher's Note